

# Majorana corner modes and flat-band Majorana edge modes in superconductor/topological-insulator/superconductor junctions

Xiao-Ting Chen,<sup>1,\*</sup> Chun-Hui Liu,<sup>2,3,\*</sup> Dong-Hui Xu,<sup>4,5,†</sup> and Chui-Zhen Chen<sup>1,‡</sup>

<sup>1</sup>*Institute for Advanced Study and School of Physical Science and Technology, Soochow University, Suzhou 215006, China.*

<sup>2</sup>*Beijing National Laboratory for Condensed Matter Physics,  
Institute of Physics, Chinese Academy of Sciences, Beijing 100190, China*

<sup>3</sup>*School of Physical Sciences, University of Chinese Academy of Sciences, Beijing 100049, China*

<sup>4</sup>*Department of Physics and Chongqing Key Laboratory for Strongly Coupled Physics, Chongqing University, Chongqing 400044, China*

<sup>5</sup>*Center of Quantum Materials and Devices, Chongqing University, Chongqing 400044, China*

Recently, superconductors with higher-order topology have stimulated extensive attention and research interest. Higher-order topological superconductors exhibit unconventional bulk-boundary correspondence, thus allow exotic lower-dimensional boundary modes, such as Majorana corner and hinge modes. However, higher-order topological superconductivity has yet to be found in naturally occurring materials. In this work, we investigate higher-order topology in a two-dimensional Josephson junction comprised of two  $s$ -wave superconductors separated by a topological insulator thin film. We found that zero-energy Majorana corner modes, a boundary fingerprint of higher-order topological superconductivity, can be achieved by applying magnetic field. When an in-plane Zeeman field is applied to the system, two corner modes appear in the superconducting junction. Furthermore, we also discover a two dimensional nodal superconducting phase which supports flat-band Majorana edge modes connecting the bulk nodes. Importantly, we demonstrate that zero-energy Majorana corner modes are stable when increasing the thickness of topological insulator thin film.

## I. INTRODUCTION

The search for topological superconductors which host Majorana zero-energy modes has been one of the central subjects in condensed matter physics [1–6], since they provide an ideal platform to potential applications in quantum computations based on non-Abelian statistics [7–13]. In 2001, A.Y. Kitaev proposed to realize Majorana zero-energy modes at the ends of one-dimensional  $p$ -wave superconductors [14]. Experimentally, the signatures of zero-energy modes were reported to be observed in spin-orbital coupled semiconductor wires in proximity to  $s$ -wave superconductors [15–18] and in the vortex of the iron-based superconductor [19–23]. However, conclusive identification of Majorana zero energy modes and scalable fabrication of Majorana networks remain challenging [5, 6, 24].

Recently, higher-order topological phases of matter, such as the higher-order topological insulators and higher-order topological superconductors have been identified as a novel topological state, which feature the unconventional bulk-boundary correspondence [25–46]. Generally, the  $n$ th higher-order topological superconductors in  $d$  dimensions support  $(d - n)$  dimensional gapless boundary excitations with  $2 \leq n \leq d$  [27, 47–85], which is in contrast to the  $d$  dimensional conventional topological superconductors with  $(d - 1)$  dimensional boundary excitations [1, 2, 86, 87]. In this endeavor, Majorana zero-energy modes are supposed to be localized at the corners of a two dimensional second-order topological superconductor (SOTSC) [27, 48–50, 53, 57, 72, 75]. Due to naturally occurring topological superconductors are extremely

rare, SOTSCs with Majorana Kramers pairs of zero modes or single Majorana zero mode at a corner have been proposed in artificial materials, such as a quantum spin Hall insulators (QSHI) in proximity to a  $d$ -wave or an  $s_{\pm}$ -wave superconductor [48, 49], two coupled chiral  $p$ -wave superconductors [50], Rashba spin-orbit coupled  $\pi$ -junction [56], etc. However, the experimental implementation remains challenging because of the requirements of ideal helical-edge modes of the QSHI, unconventional superconductivities or complicated junction. Fortunately, topological insulator thin films/ $s$ -wave superconductors hybrid structures have been successfully fabricated [88–90] and used to engineer the first-order topological superconductors [91, 92]. Even more importantly, a spin-selective Andreev reflection in the vortex of topological insulator/superconductor heterostructure was reported in a scanning tunnel microscope measurement [93], which is regarded as a fingerprint of Majorana zero-energy modes.

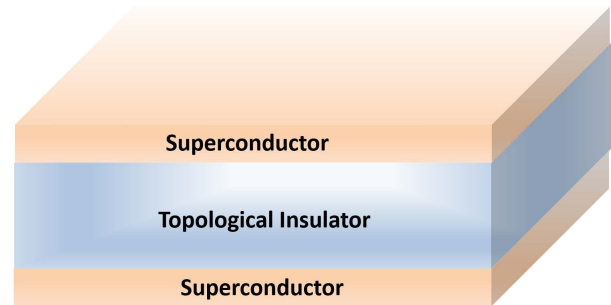


FIG. 1. (Color online). Schematic plots of topological insulator multilayer based superconductor junction.

In this work, we propose that a topological insulator thin film sandwiched between two  $s$ -wave superconductors with a phase difference  $\pi$  (see Fig. 1) can realize an SOTSC with two localized Majorana corner modes when apply-

\* These authors contributed equally to this work.

† donghuixu@cqu.edu.cn

‡ czchen@suda.edu.cn

ing an in-plane magnetic field. Moreover, a nodal topological superconducting phase hosting flat-band Majorana edge modes emerges when tuning the magnetic field. We also show that Majorana corner modes exist when varying the number of layers of topological insulator thin film. Our findings make the superconductor-topological-insulator-superconductor junctions an incredibly fertile platform for exploring topological superconducting phase.

The structure of this paper is as follows. In Sec. II we describe our setup, which consists of a topological insulator thin film, in proximity to a top and a bottom superconductors with a phase difference of  $\pi$ , see Fig. 1. In Sec. III, we present the Majorana corner modes and flat-band Majorana edge modes, and plot a topological superconducting phase diagram. Meanwhile, we do the symmetry analysis and calculate topological invariants to characterize the topological superconducting phases. We also construct an edge theory based on the perturbation theory to elucidate the formation of Majorana corner modes. In Sec. IV, We study how the thickness of topological insulator thin film affects the zero-energy Majorana corner modes. We summarize our results in Sec. V.

## II. MODEL

In reciprocal space, the effective Hamiltonian of the superconductor/topological-insulator/superconductor heterostructure can be written as

$$H(\mathbf{k}) = \frac{A}{a} \sin(k_x a) \sigma_x \tau_z + \frac{A}{a} \sin(k_y a) \rho_z \sigma_y \tau_z + M(\mathbf{k}) \rho_z \tau_x + \Delta \rho_y \sigma_y \tau_z + V_x \rho_z \sigma_x - \mu \rho_z, \quad (1)$$

in the Nambu basis  $C_{\mathbf{k}} = (c_{\mathbf{k}l,\uparrow}, c_{\mathbf{k}l,\downarrow}, c_{-\mathbf{k}l,\uparrow}^\dagger, c_{-\mathbf{k}l,\downarrow}^\dagger)^T$ , where  $\uparrow$  and  $\downarrow$  represent two electron spin directions, and  $l = 1, 2$  is the layer index.  $\sigma_i, \tau_i$  and  $\rho_i$  ( $i = x, y, z$ ) are the Pauli matrices. In Eq. (1), they acting on the spin, layer, and particle-hole spaces, respectively.  $\sigma_0, \tau_0$  and  $\rho_0$  are the  $2 \times 2$  identity matrices.  $M(\mathbf{k}) = m_0 - \frac{2m_1}{a^2} [2 - \cos(k_x a) - \cos(k_y a)]$  describes the mass induced by the hybridization of the top and bottom surfaces of the topological insulator thin film.  $A$  is the characteristic parameter of the kinetic energy of the Dirac fermions, and  $\mu$  denotes the chemical potential.  $\Delta$  is the  $s$ -wave pairing amplitude, and the pairing functions of the top and bottom surfaces of the thin film have opposite sign, which makes the setup a Josephson junction with a  $\pi$  phase shift.  $V_x$  represents the in-plane Zeeman field applied along the  $x$  direction. We set the lattice constant  $a = 5$  nm,  $A = 300$  meV  $\cdot$  nm and  $m_1 = 150$  meV  $\cdot$  nm<sup>2</sup> [94]. For our purpose, we set  $m_0 = -2$  meV and  $\Delta = 2$  meV in this case.

Before turning to discuss the Majorana corner modes in this junction, we would like to give a brief discussion about the case without applied magnetic field. In this case, time-reversal symmetry restores, a topological superconducting phase with gapless helical Majorana edge modes [see Fig. 2(a)] exists when  $m_0^2 < \Delta^2 + \mu^2$  [92]. The helical edge modes are confirmed by calculating the Bogoliubov quasiparticle energy spectrum and the local density of states for a square nanodisk, which are shown in Figs. 2(d) and 2(g).

## III. MAJORANA CORNER MODES AND FLAT-BAND EDGE MODES

When turning on the in-plane Zeeman field, we find that the gapless helical Majorana edge modes are not stable owing to time-reversal symmetry breaking, in the meantime, an energy gap opens as shown in Fig. 2(b). This gap signals the occurrence of the SOTSC. We compute the Bogoliubov quasiparticle spectrum for a finite-sized sample with a rhombus geometry. The spectrum depicted in Fig. 2(e) shows two degenerate Majorana ingap bound states at zero energy, which reside at the top and bottom corners of the rhombus, respectively, as depicted in Fig. 2(h). These two Majorana corner modes are a smoking-gun signature of the SOTSC. In the following, we will construct a topological invariant and an edge theory based on the Jackiw-Rebbi mechanism to characterize the zero-energy Majorana corner modes in SOTSC phase.

The Hamiltonian maintains the mirror symmetry:  $C_{2y} H(k_x, k_y) C_{2y}^{-1} = H(-k_x, k_y)$  with  $C_{2y} = i \sigma_x \tau_x$ . Along the mirror invariant axis  $k_x = 0$  of the first Brillouin zone (BZ),  $H(k_x = 0, k_y)$  commutes with  $C_{2y}$  operator. We can use a mirror winding number along this axis to characterize the topological properties of the Majorana corner modes [70, 95, 96]. The expression of  $H(k_x = 0, k_y)$  is

$$H(0, k_y) = \frac{A}{a} \sin(k_y a) \rho_z \sigma_y \tau_z + M(0, k_y) \rho_z \tau_x + \Delta \rho_y \sigma_y \tau_z + V_x \rho_z \sigma_x - \mu \rho_z, \quad (2)$$

where  $M(0, k_y) = m_0 - \frac{2m_1}{a^2} [1 - \cos(k_y a)]$ .  $C_{2y}$  has two fourfold degenerate eigenvalues of  $\pm 1$ . The eigenvectors with eigenvalue of  $+1$  are:

$$\begin{aligned} \chi_1 &= |\rho_z = 1, \sigma_x = 1, \tau_x = 1\rangle, \\ \chi_2 &= |\rho_z = -1, \sigma_x = 1, \tau_x = 1\rangle, \\ \chi_3 &= |\rho_z = 1, \sigma_x = -1, \tau_x = -1\rangle, \\ \chi_4 &= |\rho_z = -1, \sigma_x = -1, \tau_x = -1\rangle, \end{aligned} \quad (3)$$

which constitutes the  $+1$  eigenspace. The eigenvectors with eigenvalue of  $-1$  are:

$$\begin{aligned} \chi_5 &= |\rho_z = 1, \sigma_x = 1, \tau_x = -1\rangle, \\ \chi_6 &= |\rho_z = -1, \sigma_x = 1, \tau_x = -1\rangle, \\ \chi_7 &= |\rho_z = 1, \sigma_x = -1, \tau_x = 1\rangle, \\ \chi_8 &= |\rho_z = -1, \sigma_x = -1, \tau_x = 1\rangle, \end{aligned} \quad (4)$$

which constitutes the  $-1$  eigenspace. Projecting  $H(0, k_y)$  into  $+1$  eigenspace ( $-1$  eigenspace) of  $C_{2y}$ , we can get a Hamiltonian in the subspace  $H_+(0, k_y)$  [ $H_-(0, k_y)$ ]. Using  $\chi_1, \chi_2, \dots, \chi_8$  as a new basis set of Hilbert space, we can get  $H(0, k_y) = H_+(0, k_y) \oplus H_-(0, k_y)$  with

$$H_{\pm}(0, k_y) = \mp \frac{A}{a} \sin(k_y a) \rho_z \sigma_y + M(0, k_y) \rho_z \sigma_z \mp \Delta \rho_y \sigma_y \pm V_x \rho_z \sigma_x - \mu \rho_z. \quad (5)$$

In the first BZ, we can define the Wilson loop operator  $W_{\pm, k_y}$  of  $H_{\pm}(0, k_y)$ , along the mirror-invariant axis  $k_x = 0$ . The

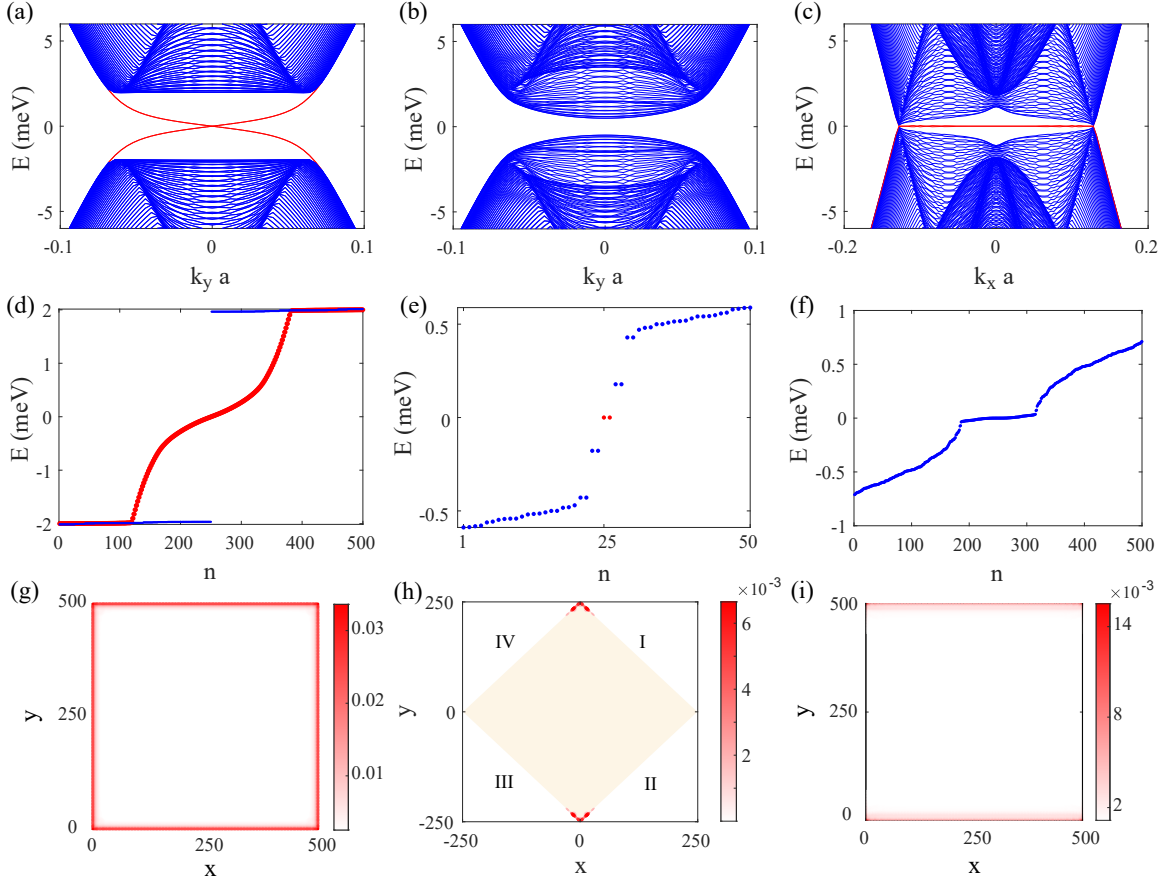


FIG. 2. (Color online). Energy dispersion of a ribbon geometry for (a)  $V_x = 0$  meV, (b)  $V_x = 1.5$  meV, (c)  $V_x = 12$  meV. In (a) and (b), we take the open boundary condition in the  $x$ -direction. In (c), we take the open boundary condition in the  $y$ -direction as the bulk nodes are located along the  $k_x$ -axis. (d) Blue (red) dots are energy spectrum of the configuration in (g) under the periodic boundary condition (open boundary condition) in all boundaries, the parameters the same as (a). (e) The energy spectrum of the configuration in (h) with the open boundary condition in all boundaries, the parameters the same as (b). (f) The energy spectrum of configuration in (i) with the open boundary condition in the  $y$ -direction and the periodic boundary condition in the  $x$ -direction, the parameters the same as (c). (g) Local density of states of gapless Majorana edge modes in (d). (h) Local density states of the ingap Majorana bound states at zero energy marked in red in (e). (i) Local density of flat-band edge modes in (f). In (a)-(i), the parameters are  $\mu = 12$  meV,  $\Delta = 2$  meV.

mirror winding number  $\nu_{\pm}$  can be written as [95, 96]:

$$\nu_{\pm} = \frac{1}{i\pi} \log(\det[W_{\pm, k_y}]) \bmod 2. \quad (6)$$

When corner modes occur, the mirror winding number  $\nu_+ = \nu_- = 1$  [70].

Next, we use degenerate perturbation theory to deduce the SOTSC phase. For simplicity, we only consider  $\mu = 0$ , and  $V_x$  terms are small enough such that they can be treated as perturbations. The low energy expansion of the SOTSC Hamiltonian in Eq. (1) at  $\mathbf{k} = (0, 0)$  is

$$H_l = Ak_x \sigma_x \tau_z + Ak_y \rho_z \sigma_y \tau_z + [m_0 - m_1(k_x^2 + k_y^2)] \rho_z \tau_x + \Delta \rho_y \sigma_y \tau_z + V_x \rho_z \sigma_x, \quad (7)$$

Define new momenta

$$\tilde{k}_x = \frac{k_x + k_y}{\sqrt{2}}, \quad \tilde{k}_y = \frac{k_x - k_y}{\sqrt{2}} \quad (8)$$

which are parallel to the border of the rhombus-shaped sample in Fig. 2(h). Through these new momenta, the  $H_l$  can be represented as

$$H_l = \frac{A}{\sqrt{2}}(\tilde{k}_x + \tilde{k}_y) \sigma_x \tau_z + \frac{A}{\sqrt{2}}(\tilde{k}_x - \tilde{k}_y) \rho_z \sigma_y \tau_z + [m_0 - m_1(\tilde{k}_x^2 + \tilde{k}_y^2)] \rho_z \tau_x + \Delta \rho_y \sigma_y \tau_z + V_x \rho_z \sigma_x, \quad (9)$$

Consider the open boundary condition in the  $\frac{1}{\sqrt{2}}(1, 1)$  direction and periodic boundary condition in the  $\frac{1}{\sqrt{2}}(1, -1)$  direction, we also can treat  $\tilde{k}_y$  term as perturbation. After omitting the high-order perturbation  $O(\tilde{k}_y^2)$  term, we have  $H_l = H_0 + H_p$  with

$$H_0 = \frac{A}{\sqrt{2}} \tilde{k}_x \sigma_x \tau_z + \frac{A}{\sqrt{2}} \tilde{k}_x \rho_z \sigma_y \tau_z + [m_0 - m_1 \tilde{k}_x^2] \rho_z \tau_x + \Delta \rho_y \sigma_y \tau_z \quad (10)$$

$$H_p = \frac{A}{\sqrt{2}} \tilde{k}_y \sigma_x \tau_z - \frac{A}{\sqrt{2}} \tilde{k}_y \rho_z \sigma_y \tau_z + V_x \rho_z \sigma_x. \quad (11)$$

We treat  $H_0$  as unperturbed Hamiltonian and  $H_p$  as perturbation. Notice that  $[H_0, \rho_x \sigma_x \tau_z] = [H_0, \rho_x \sigma_y \tau_y] = 0$ ,  $\rho_x \sigma_x \tau_z$  has eigenvectors

$$\begin{aligned} \psi_1 &= |\rho_x = 1, \sigma_x = 1, \tau_z = 1\rangle \\ \psi_2 &= |\rho_x = 1, \sigma_x = -1, \tau_z = -1\rangle \\ \psi_3 &= |\rho_x = -1, \sigma_x = 1, \tau_z = -1\rangle \\ \psi_4 &= |\rho_x = -1, \sigma_x = -1, \tau_z = 1\rangle \\ \psi_5 &= |\rho_x = 1, \sigma_x = 1, \tau_z = -1\rangle \\ \psi_6 &= |\rho_x = 1, \sigma_x = -1, \tau_z = 1\rangle \\ \psi_7 &= |\rho_x = -1, \sigma_x = 1, \tau_z = 1\rangle \\ \psi_8 &= |\rho_x = -1, \sigma_x = -1, \tau_z = -1\rangle \end{aligned} \quad (12)$$

$\rho_x \sigma_x \tau_z$  and  $\rho_x \sigma_y \tau_y$  have common eigenvectors

$$\begin{aligned} \chi_1 &= \frac{1}{\sqrt{2}}(\psi_1 + \psi_2), & \chi_2 &= \frac{1}{\sqrt{2}}(\psi_3 + \psi_4) \\ \chi_3 &= \frac{1}{\sqrt{2}}(\psi_1 - \psi_2), & \chi_4 &= \frac{1}{\sqrt{2}}(\psi_3 - \psi_4) \\ \chi_5 &= \frac{1}{\sqrt{2}}(\psi_5 - \psi_6), & \chi_6 &= \frac{1}{\sqrt{2}}(\psi_7 - \psi_8) \\ \chi_7 &= \frac{1}{\sqrt{2}}(\psi_5 + \psi_6), & \chi_8 &= \frac{1}{\sqrt{2}}(\psi_7 + \psi_8) \end{aligned} \quad (13)$$

Using these basis, we can define a unitary transformation

$$U_1 = [\chi_1, \chi_2, \chi_3, \chi_4, \chi_5, \chi_6, \chi_7, \chi_8]. \quad (14)$$

We remark that  $\mathbf{s}$ ,  $\boldsymbol{\sigma}$ , and  $\boldsymbol{\tau}$  only represent Pauli matrix in orthogonal space. Consider the rotation of Pauli  $\boldsymbol{\tau}$  space, we can define another unitary transformation

$$U_2 = e^{i\pi\tau_z/8}. \quad (15)$$

Under these two unitary transformations, we can get new  $H_I$ ,  $H_0$ , and  $H_p$ , labeled as  $H_I^n$ ,  $H_0^n$ , and  $H_p^n$ , respectively, with

$$\begin{aligned} H_0^n(\tilde{k}_x) &= U_2^\dagger U_1^\dagger H_0 U_1 U_2 \\ &= \text{diag} \left[ -A\tilde{k}_x \tau_y + (m_0 - \Delta - m_1 \tilde{k}_x^2) \tau_x, \right. \\ &\quad A\tilde{k}_x \tau_z + (m_0 + \Delta - m_1 \tilde{k}_x^2) \tau_x, \\ &\quad -A\tilde{k}_x \tau_z + (m_0 - \Delta - m_1 \tilde{k}_x^2) \tau_x, \\ &\quad \left. A\tilde{k}_x \tau_y + (m_0 + \Delta - m_1 \tilde{k}_x^2) \tau_x \right], \end{aligned} \quad (16)$$

$$\begin{aligned} H_p^n &= U_2^\dagger U_1^\dagger H_p U_1 U_2 \\ &= \frac{A}{2} \tilde{k}_y (\rho_z \tau_z - \rho_z \tau_y + \sigma_z \tau_z + \sigma_z \tau_y) + V_x \rho_x \tau_x \end{aligned} \quad (17)$$

and  $H_I^n = H_0^n + H_p^n$ . Substitute  $\tilde{k}_x$  with  $-i\partial_{\tilde{x}}$ , we get the zero modes equation  $H_0^n(-i\partial_{\tilde{x}})\phi_\alpha = 0$ . When  $|\Delta| > |m_0|$

and  $m_1 < 0$ , there are two zero energy solutions on the I edge of Fig. 2(h):  $\phi_\alpha = N_{\tilde{x}} \sin(\kappa_1 \tilde{x}) e^{\kappa_2 \tilde{x}} e^{i\tilde{k}_y \tilde{y}} \xi_\alpha$

$$\begin{aligned} \xi_1 &= |\rho_z = 1, \sigma_z = 1, \tau_z = -1\rangle \\ \xi_2 &= |\rho_z = -1, \sigma_z = 1, \tau_y = 1\rangle, \end{aligned} \quad (18)$$

$\kappa_1 = \frac{\sqrt{4(m_0 - \Delta)m_1 - A^2}}{2m_1}$ ,  $\kappa_2 = \frac{A}{2|m_1|}$ , and  $N_{\tilde{x}} = \frac{2\kappa_2 \sqrt{(\kappa_1^2 + \kappa_2^2)}}{\kappa_1}$ .  $\tilde{x}$  and  $\tilde{y}$  are the coordinates along  $\frac{1}{\sqrt{2}}(1, 1)$  and  $\frac{1}{\sqrt{2}}(1, -1)$  directions, respectively. Under  $\phi_\alpha$  ( $\alpha = 1, 2$ ),  $H_p^n$  can be written as

$$H_I = -A\tilde{k}_y \sigma_z + \frac{V_x}{2} \sigma_x \quad (19)$$

In same vein, we can deduce the effective Hamiltonian on III, II, and IV edges

$$\begin{aligned} H_{III} &= A\tilde{k}_y \sigma_z - \frac{V_x}{2} \sigma_x \\ H_{II} &= A\tilde{k}_x \sigma_z + \frac{V_x}{2} \sigma_x \\ H_{IV} &= -A\tilde{k}_x \sigma_z - \frac{V_x}{2} \sigma_x \end{aligned} \quad (20)$$

$H_I$ ,  $H_{II}$ ,  $H_{III}$ , and  $H_{IV}$  are the Jackiw-Rebbi model [97] describing Dirac equation subjected to a mass kink. Accordingly, we deduce that there are zero mode at the corner of II and III edges as well as the corner of IV and I edges, as around each of the two corners the Dirac equation on two adjacent edges gain the opposite-sign mass.

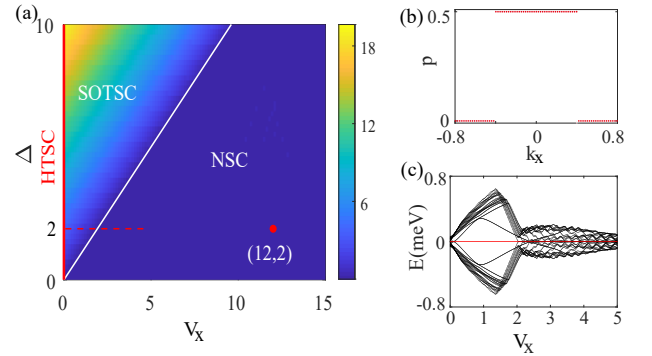


FIG. 3. (Color online). (a) Phase diagram of topological superconductors. The upper left regime marked by SOTSC represents the second-order topological superconductor phase. The lower right regime marked by NSC represents the nodal topological superconductor phase. The left red solid line represents the helical topological superconductor (HTSC) phase in the absence of  $V_x$ . The color bar represents the energy gap. (b) Bulk polarization of the nodal phase as a function of  $k_x$ . In (a) and (b), we fix  $\mu = 12$  meV. In (b), we also fix  $\Delta_t = 2$  meV and  $M_x = 1.5$  meV. (c) Energy spectrum as a function of  $V_x$  for a finite-sized sample with rhombus geometry. The parameters correspond to the red dashed line in (a).

Continuing to increase the in-plane Zeeman field  $V_x$ , we find that the gap closes, and a nodal topological superconducting phase with nodes along the  $k_x$ -axis is formed. Considering

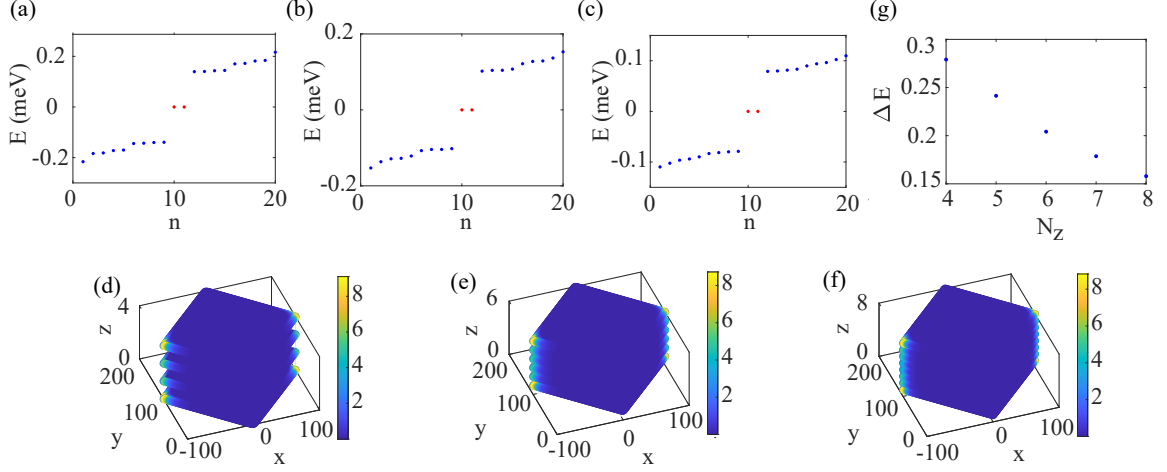


FIG. 4. (Color online).  $N_x \times N_y = 200 \times 200$  and rhombus-shaped sample for all plots. The energy spectrum for distinct number of layers (a)  $N_z = 4$ , (b)  $N_z = 6$ , and (c)  $N_z = 8$ . (d), (e), and (f) are the local density of the two Majorana ingap bound states marked in red dots in (a), (b), and (c), respectively. (g) The gap of bulk spectrum marked in blue dots as a function of number of layers  $N_z$ . In (a)-(g), we set  $a = 5$  nm,  $A = 50$  meV  $\cdot$  nm,  $m_0 = 8$  meV,  $\mu = 2$  meV,  $\Delta = 2$  meV,  $V_x = 1.5$  meV,  $t_x = t_y = 125$  meV  $\cdot$  nm<sup>2</sup> and  $t_z = 100$  meV  $\cdot$  nm<sup>2</sup>.

a ribbon geometry with the open boundary condition along  $y$  direction, we plot the energy spectrum in Fig. 2(c). Clearly, this nodal phase hosts flat-band Majorana edge modes between the two bulk nodes. The flat-band Majorana edge modes are confirmed by calculating the energy spectrum and the local density of states of the edge modes, displayed in Figs. 2(f) and 2(i). We can see that the flat-band Majorana edge modes are located on the top and bottom edges of the sample.

To capture the topological characteristic of the nodal phase, we further adopt the Wilson loop method [28, 29, 33, 98–101] to calculate the bulk polarization of the system. Since the bulk nodes are located along the  $k_x$ -axis, by treating  $k_x$  as a parameter, the effective Hamiltonian reduces to a one-dimensional Hamiltonian  $H_{k_x}(k_y)$ . The Wilson loop operator [28, 29, 33, 98–101] along the path in the  $k_y$ -direction  $W_{y,k_y}$  is defined by:  $W_{y,k_y} = F_{y,k_y+(N_y-1)\Delta k_y} \cdots F_{y,k_y+\Delta k_y} F_{y,k_y}$ , where  $k_y$  is the base point and  $N_y$  is the number of unit cells in the  $y$ -direction. Here,  $[F_{y,k_y}]^{mn} = \langle u_{k_y+\Delta k_y}^m | u_{k_y}^n \rangle$  with the step  $\Delta k_y = 2\pi/N_y$ , and  $|u_{k_y}^n\rangle$  represents the occupied Bloch wave functions with  $n = 1, 2, \dots, N_{\text{occ}}$ .  $N_{\text{occ}} = N_b/2$  is the number of occupied bands, with  $N_b$  the degrees of freedom for each cell. Fixing  $k_x$ , we can determine the Wilson loop operator  $W_{y,k_y}$  on a path along  $k_y$ . The Wannier center  $v_y^j$  can be determined by the eigenvalues of the Wilson-loop operator  $W_{y,k_y}$ ,

$$W_{y,k_y} |v_{y,k_y}^j\rangle = e^{i2\pi v_y^j} |v_{y,k_y}^j\rangle, \quad (21)$$

where  $j \in \{1, 2, \dots, N_{\text{occ}}\}$  labels eigenstates  $|v_{y,k_y}^j\rangle$  as well as components  $[v_{y,k_y}^j]^n$ . Since  $k_x$  is fixed, the bulk polarization can be defined as  $p = \sum_j v_y^j \bmod 1$  [28]. We plot the bulk polarization as a function of  $k_x$  as shown in Fig. 3(b). It is clear that the polarization is quantized to 1/2 between two nodal points. We remark that the topological characteristic of

the nodal phase can be portrayed by the  $k_x$ -dependent polarization.

Finally, we plot the topological superconducting phase diagram on the plane of  $\Delta$  and  $V_x$  as shown in Fig. 3(a). The phase boundaries are determined by numerically observing the gap closure of the bulk. The phase boundary between SOTSC and the nodal topological superconductor (NSC) is approximately fitted by the line  $V_x = \Delta$ . By tuning the in-plane Zeeman field  $V_x$ , SOTSC phase, NSC phase, and helical topological superconductor (HTSC) phase can be achieved. Figure 3(c) shows the energy spectrum as a function of  $V_x$  for the finite-sized sample with rhombus-like geometry in Fig. 2(h).

#### IV. THE EFFECT OF THICKNESS ON MAJORANA CORNER MODES

In this section, we study how the thickness of the topological insulator thin film affects the Majorana corner modes. In the three-dimensional limit, the bulk Hamiltonian of the intermediate topological insulator can be expressed as:

$$H_{3\text{DTI}}(\mathbf{k}) = \frac{A}{a} \sin(k_x a) \sigma_x \tau_x + \frac{A}{a} \sin(k_y a) \sigma_y \tau_x - \mu + \frac{A}{a} \sin(k_z a) \sigma_z \tau_x + M(\mathbf{k}) \tau_z + V_x \sigma_x, \quad (22)$$

where  $M(\mathbf{k}) = m_0 - 2\frac{t_x}{a^2}(1 - \cos(k_x a)) - 2\frac{t_y}{a^2}(1 - \cos(k_y a)) - 2\frac{t_z}{a^2}(1 - \cos(k_z a))$  with  $\mathbf{k} = (k_x, k_y, k_z)$ , and  $V_x$  is the Zeeman field along the  $x$ -direction. For simplicity, we consider the proximity-induced superconducting gap only exists on the outermost layers of the top and bottom surfaces of the three-dimensional topological insulator, and the top and bottom superconductors remain a  $\pi$  phase shift. In reality, the proximity-induced superconducting potential decreases exponentially and can extend to several layers [88, 90].

However, this will not change the physics discussed in this section. Considering the confinement of the topological insulator thin film along the  $z$ -direction, the total Hamiltonian in the Nambu space can be written as,

$$\begin{aligned}
H_{3D}(\mathbf{k}_{\parallel}) = & \sum_{z=1}^{N_z-1} b_{\mathbf{k}_{\parallel},z}^{\dagger} \left( -\frac{iA}{2} \sigma_z \tau_x + t_z \rho_z \tau_z \right) b_{\mathbf{k}_{\parallel},z+1} + \text{h.c.} \\
& + \sum_{z=1}^{N_z} b_{\mathbf{k}_{\parallel},z}^{\dagger} [A \sin(k_x a) \sigma_x \tau_x + A \sin(k_y a) \rho_y \sigma_y \tau_x \\
& + V_x \rho_z \sigma_x - \mu \rho_z + \tilde{M}(\mathbf{k}_{\parallel}) \rho_z \tau_z] b_{\mathbf{k}_{\parallel},z} \\
& + (b_{\mathbf{k}_{\parallel},1}^{\dagger} \Delta \rho_y \sigma_y b_{\mathbf{k}_{\parallel},1} - b_{\mathbf{k}_{\parallel},N_z}^{\dagger} \Delta \rho_y \sigma_y b_{\mathbf{k}_{\parallel},N_z}),
\end{aligned} \tag{23}$$

where  $b_{\mathbf{k}_{\parallel},z} = [\psi_{l,\alpha}(\mathbf{k}_{\parallel}, z), \psi_{l,\alpha}^{\dagger}(-\mathbf{k}_{\parallel}, z)]^T$  with the orbital index  $l = P1$  ( $P2$ ) and the spin index  $\alpha = \uparrow$  ( $\downarrow$ ).  $\tilde{M}(\mathbf{k}_{\parallel}) = m_0 - 2t_x(1 - \cos(k_x a)) - 2t_y(1 - \cos(k_y a)) - 2t_z/a^2$  and  $\mathbf{k}_{\parallel} = (k_x, k_y)$ . Generally, the low energy physics of the topological insulator thin film  $H_{3D}(\mathbf{k}_{\parallel})$  can be described by the 2D Hamiltonian  $H(\mathbf{k})$  in Eq. (1) [102]. Similar to  $H(\mathbf{k})$ , the Hamiltonian  $H_{3D}(\mathbf{k}_{\parallel})$  preserves the mirror-like symmetry:  $C_{2y} H_{3D}(k_x, k_y) C_{2y}^{-1} = H_{3D}(-k_x, k_y)$  with  $C_{2y} = i\sigma_x \mathcal{U}$ . Here  $N_x \times N_y$  anti-diagonal matrix  $\mathcal{U}_{ij} = \delta_{i+j, N_x+1}$  is defined in real space with Kronecker delta  $\delta_{i,j}$ . Thereore, it is natural to expect the Majorana corner modes will be sustainable with the varying thickness. For  $\Delta \neq 0$ ,  $V_x = 0$ , the system is a helical topological superconductor, if the Fermi energy is outside the surface gap [92]. By turning on the Zeeman field  $V_x > 0$ , the gapless Majorana corner modes are observed, as shown in Fig. 4. Figures 4(a), 4(b), and 4(c) show the energy spectrum (only the 20 eigenenergies with the smallest absolute value are shown) of an  $N_x \times N_y = 200 \times 200$  rhombus-shaped sample. Again, two zero-energy ingap Majorana bound states appear (marked by the red dots in Fig. 4). Figures 4(d), 4(e), and 4(f)

are the local density of the two zero-energy Majorana bound states in Figs. 4(a), 4(b), and 4(c), respectively. We can see that the two Majorana bound states are also localized at two opposite corners in the  $xy$ -plane, but extended in hinge of the side surface along the  $z$ -direction. In order to explore the relationship between the gap of side-surface spectrum [marked in blue dots in Figs. 4(a)-4(c)] and the number of layers  $N_z$ , we plot the band gap for different number of layers  $N_z$  in Fig. 4(g). It implies that the band gap decreases rapidly with the increase of  $N_z$  due to the decreasing finite-size confinement along the  $z$ -direction.

## V. CONCLUSIONS

In conclusion, we have illustrated that an SOTSC with two Majorana corner modes is realized in topological insulator thin film based superconducting junctions with a  $\pi$  phase shift when an in-plane Zeeman field is applied. We employ the mirror winding number to characterize the second-order topology of Majorana corner modes. We also analytically deduce an edge theory for the Majorana corner modes by using the perturbation theory. By tuning the Zeeman field, we also observe a nodal superconducting phase hosting flat-band Majorana edge modes, whose bulk topology can be captured by a  $k$ -dependent polarization. At last, we demonstrate that how the thickness of topological insulator thin films affects the Majorana corner modes and their spatial distribution.

## ACKNOWLEDGMENTS

The authors acknowledge the support by the NSFC (under Grants No. 12074108, No. 11974256, and No.12147102), and the Priority Academic Program Development (PAPD) of Jiangsu Higher Education Institution.

- 
- [1] M. Z. Hasan and C. L. Kane, Colloquium: Topological insulators, *Rev. Mod. Phys.* **82**, 3045 (2010).
  - [2] X.-L. Qi and S.-C. Zhang, Topological insulators and superconductors, *Rev. Mod. Phys.* **83**, 1057 (2011).
  - [3] J. Alicea, New directions in the pursuit of majorana fermions in solid state systems, *Reports on progress in physics* **75**, 076501 (2012).
  - [4] C. Beenakker, Search for majorana fermions in superconductors, *Annu. Rev. Condens. Matter Phys.* **4**, 113 (2013).
  - [5] R. M. Lutchyn, E. P. Bakkers, L. P. Kouwenhoven, P. Krogstrup, C. M. Marcus, and Y. Oreg, Majorana zero modes in superconductor–semiconductor heterostructures, *Nature Reviews Materials* **3**, 52 (2018).
  - [6] K. Flensberg, F. von Oppen, and A. Stern, Engineered platforms for topological superconductivity and majorana zero modes, *Nature Reviews Materials* **6**, 944 (2021).
  - [7] D. A. Ivanov, Non-abelian statistics of half-quantum vortices in  $p$ -wave superconductors, *Phys. Rev. Lett.* **86**, 268 (2001).
  - [8] A. Y. Kitaev, Fault-tolerant quantum computation by anyons, *Annals of Physics* **303**, 2 (2003).
  - [9] C. Nayak, S. H. Simon, A. Stern, M. Freedman, and S. Das Sarma, Non-abelian anyons and topological quantum computation, *Rev. Mod. Phys.* **80**, 1083 (2008).
  - [10] J. Alicea, Y. Oreg, G. Refael, F. von Oppen, and M. P. A. Fisher, Non-abelian statistics and topological quantum information processing in 1d wire networks, *Nature Physics* **7**, 412 (2011).
  - [11] K. Flensberg, Non-abelian operations on majorana fermions via single-charge control, *Phys. Rev. Lett.* **106**, 090503 (2011).
  - [12] B. van Heck, A. R. Akhmerov, F. Hassler, M. Burrello, and C. W. J. Beenakker, Coulomb-assisted braiding of majorana fermions in a josephson junction array, *New Journal of Physics* **14**, 035019 (2012).
  - [13] D. Aasen, M. Hell, R. V. Mishmash, A. Higginbotham, J. Danon, M. Leijnse, T. S. Jespersen, J. A. Folk, C. M. Marcus, K. Flensberg, and J. Alicea, Milestones toward majorana-based quantum computing, *Phys. Rev. X* **6**, 031016 (2016).
  - [14] A. Y. Kitaev, Unpaired majorana fermions in quantum wires, *Physics-uspekhi* **44**, 131 (2001).

- [15] V. Mourik, K. Zuo, S. M. Frolov, S. R. Plissard, E. P. A. M. Bakkers, and L. P. Kouwenhoven, Signatures of majorana fermions in hybrid superconductor-semiconductor nanowire devices, *Science* **336**, 1003 (2012).
- [16] A. Das, Y. Ronen, Y. Most, Y. Oreg, M. Heiblum, and H. Shtrikman, Zero-bias peaks and splitting in an Al-InAs nanowire topological superconductor as a signature of Majorana fermions, *Nature Physics* **8**, 887 (2012).
- [17] M. T. Deng, C. L. Yu, G. Y. Huang, M. Larsson, P. Caroff, and H. Q. Xu, Anomalous Zero-Bias Conductance Peak in a Nb-InSb Nanowire-Nb Hybrid Device, *Nano Letters* **12**, 6414 (2012).
- [18] R. M. Lutchyn, J. D. Sau, and S. Das Sarma, Majorana fermions and a topological phase transition in semiconductor-superconductor heterostructures, *Phys. Rev. Lett.* **105**, 077001 (2010).
- [19] P. Zhang, K. Yaji, T. Hashimoto, Y. Ota, T. Kondo, K. Okazaki, Z. Wang, J. Wen, G. D. Gu, H. Ding, and S. Shin, Observation of topological superconductivity on the surface of an iron-based superconductor, *Science* **360**, 182 (2018).
- [20] L. Kong, S. Zhu, M. Papaj, H. Chen, L. Cao, H. Isobe, Y. Xing, W. Liu, D. Wang, P. Fan, Y. Sun, S. Du, J. Schneeloch, R. Zhong, G. Gu, L. Fu, H.-J. Gao, and H. Ding, Half-integer level shift of vortex bound states in an iron-based superconductor, *Nature Physics* **15**, 1181 (2019), arXiv:1901.02293 [cond-mat.supr-con].
- [21] D. Wang, L. Kong, P. Fan, H. Chen, S. Zhu, W. Liu, L. Cao, Y. Sun, S. Du, J. Schneeloch, R. Zhong, G. Gu, L. Fu, H. Ding, and H.-J. Gao, Evidence for majorana bound states in an iron-based superconductor, *Science* **362**, 333 (2018).
- [22] Q. Liu, C. Chen, T. Zhang, R. Peng, Y.-J. Yan, C.-H.-P. Wen, X. Lou, Y.-L. Huang, J.-P. Tian, X.-L. Dong, G.-W. Wang, W.-C. Bao, Q.-H. Wang, Z.-P. Yin, Z.-X. Zhao, and D.-L. Feng, Robust and clean majorana zero mode in the vortex core of high-temperature superconductor  $(\text{Li}_{0.84}\text{Fe}_{0.16})\text{OHFeSe}$ , *Phys. Rev. X* **8**, 041056 (2018).
- [23] S. Zhu, L. Kong, L. Cao, H. Chen, M. Papaj, S. Du, Y. Xing, W. Liu, D. Wang, C. Shen, et al., Nearly quantized conductance plateau of vortex zero mode in an iron-based superconductor, *Science* **367**, 189 (2020).
- [24] T. Karzig, C. Knapp, R. M. Lutchyn, P. Bonderson, M. B. Hastings, C. Nayak, J. Alicea, K. Flensberg, S. Plugge, Y. Oreg, C. M. Marcus, and M. H. Freedman, Scalable designs for quasiparticle-poisoning-protected topological quantum computation with majorana zero modes, *Phys. Rev. B* **95**, 235305 (2017).
- [25] Y. Peng, Y. Bao, and F. von Oppen, Boundary green functions of topological insulators and superconductors, *Phys. Rev. B* **95**, 235143 (2017).
- [26] Z. Song, Z. Fang, and C. Fang,  $(d-2)$ -dimensional edge states of rotation symmetry protected topological states, *Phys. Rev. Lett.* **119**, 246402 (2017).
- [27] J. Langbehn, Y. Peng, L. Trifunovic, F. von Oppen, and P. W. Brouwer, Reflection-symmetric second-order topological insulators and superconductors, *Phys. Rev. Lett.* **119**, 246401 (2017).
- [28] W. A. Benalcazar, B. A. Bernevig, and T. L. Hughes, Electric multipole moments, topological multipole moment pumping, and chiral hinge states in crystalline insulators, *Phys. Rev. B* **96**, 245115 (2017).
- [29] W. A. Benalcazar, B. A. Bernevig, and T. L. Hughes, Quantized electric multipole insulators, *Science* **357**, 61 (2017).
- [30] F. Schindler, A. M. Cook, M. G. Vergniory, Z. Wang, S. S. Parkin, B. A. Bernevig, and T. Neupert, Higher-order topological insulators, *Science advances* **4**, eaat0346 (2018).
- [31] G. van Miert and C. Ortix, Higher-order topological insulators protected by inversion and rotoinversion symmetries, *Phys. Rev. B* **98**, 081110 (2018).
- [32] M. Ezawa, Strong and weak second-order topological insulators with hexagonal symmetry and  $z_3$  index, *Phys. Rev. B* **97**, 241402 (2018).
- [33] S. Franca, J. van den Brink, and I. C. Fulga, An anomalous higher-order topological insulator, *Phys. Rev. B* **98**, 201114 (2018).
- [34] M. Ezawa, Magnetic second-order topological insulators and semimetals, *Phys. Rev. B* **97**, 155305 (2018).
- [35] M. Ezawa, Higher-order topological insulators and semimetals on the breathing kagome and pyrochlore lattices, *Phys. Rev. Lett.* **120**, 026801 (2018).
- [36] M. Ezawa, Topological switch between second-order topological insulators and topological crystalline insulators, *Phys. Rev. Lett.* **121**, 116801 (2018).
- [37] F. K. Kunst, G. van Miert, and E. J. Bergholtz, Lattice models with exactly solvable topological hinge and corner states, *Phys. Rev. B* **97**, 241405 (2018).
- [38] Y. You, T. Devakul, F. J. Burnell, and T. Neupert, Higher-order symmetry-protected topological states for interacting bosons and fermions, *Phys. Rev. B* **98**, 235102 (2018).
- [39] Z. Wang, B. J. Wieder, J. Li, B. Yan, and B. A. Bernevig, Higher-order topology, monopole nodal lines, and the origin of large fermi arcs in transition metal dichalcogenides  $x\text{Te}_2$  ( $x = \text{Mo}, \text{W}$ ), *Phys. Rev. Lett.* **123**, 186401 (2019).
- [40] K. Kudo, T. Yoshida, and Y. Hatsugai, Higher-order topological mott insulators, *Phys. Rev. Lett.* **123**, 196402 (2019).
- [41] L. Trifunovic and P. W. Brouwer, Higher-order bulk-boundary correspondence for topological crystalline phases, *Phys. Rev. X* **9**, 011012 (2019).
- [42] C. Yue, Y. Xu, Z. Song, H. Weng, Y.-M. Lu, C. Fang, and X. Dai, Symmetry-enforced chiral hinge states and surface quantum anomalous hall effect in the magnetic axion insulator  $\text{Bi}_2-\text{xSb}_x\text{Se}_3$ , *Nature Physics* **15**, 577 (2019).
- [43] Y. Xu, Z. Song, Z. Wang, H. Weng, and X. Dai, Higher-order topology of the axion insulator  $\text{EuIn}_2\text{As}_2$ , *Phys. Rev. Lett.* **122**, 256402 (2019).
- [44] C.-B. Hua, R. Chen, B. Zhou, and D.-H. Xu, Higher-order topological insulator in a dodecagonal quasicrystal, *Phys. Rev. B* **102**, 241102 (2020).
- [45] R. Chen, C.-Z. Chen, J.-H. Gao, B. Zhou, and D.-H. Xu, Higher-order topological insulators in quasicrystals, *Phys. Rev. Lett.* **124**, 036803 (2020).
- [46] A. Rasmussen and Y.-M. Lu, Classification and construction of higher-order symmetry-protected topological phases of interacting bosons, *Phys. Rev. B* **101**, 085137 (2020).
- [47] M. Geier, L. Trifunovic, M. Hoskam, and P. W. Brouwer, Second-order topological insulators and superconductors with an order-two crystalline symmetry, *Phys. Rev. B* **97**, 205135 (2018).
- [48] Z. Yan, F. Song, and Z. Wang, Majorana corner modes in a high-temperature platform, *Phys. Rev. Lett.* **121**, 096803 (2018).
- [49] Q. Wang, C.-C. Liu, Y.-M. Lu, and F. Zhang, High-temperature majorana corner states, *Phys. Rev. Lett.* **121**, 186801 (2018).
- [50] X. Zhu, Tunable majorana corner states in a two-dimensional second-order topological superconductor induced by magnetic fields, *Phys. Rev. B* **97**, 205134 (2018).
- [51] E. Khalaf, Higher-order topological insulators and superconductors protected by inversion symmetry, *Phys. Rev. B* **97**, 205136 (2018).

- [52] Y. Wang, M. Lin, and T. L. Hughes, Weak-pairing higher order topological superconductors, *Phys. Rev. B* **98**, 165144 (2018).
- [53] T. Liu, J. J. He, and F. Nori, Majorana corner states in a two-dimensional magnetic topological insulator on a high-temperature superconductor, *Phys. Rev. B* **98**, 245413 (2018).
- [54] C.-H. Hsu, P. Stano, J. Klinovaja, and D. Loss, Majorana Kramers pairs in higher-order topological insulators, *Phys. Rev. Lett.* **121**, 196801 (2018).
- [55] H. Shapourian, Y. Wang, and S. Ryu, Topological crystalline superconductivity and second-order topological superconductivity in nodal-loop materials, *Phys. Rev. B* **97**, 094508 (2018).
- [56] Y. Volpez, D. Loss, and J. Klinovaja, Second-order topological superconductivity in  $\pi$ -junction rashba layers, *Phys. Rev. Lett.* **122**, 126402 (2019).
- [57] X.-H. Pan, K.-J. Yang, L. Chen, G. Xu, C.-X. Liu, and X. Liu, Lattice-symmetry-assisted second-order topological superconductors and majorana patterns, *Phys. Rev. Lett.* **123**, 156801 (2019).
- [58] S. Franca, D. V. Efremov, and I. C. Fulga, Phase-tunable second-order topological superconductor, *Phys. Rev. B* **100**, 075415 (2019).
- [59] D. Varjas, A. Lau, K. Pöyhönen, A. R. Akhmerov, D. I. Pikulin, and I. C. Fulga, Topological phases without crystalline counterparts, *Phys. Rev. Lett.* **123**, 196401 (2019).
- [60] Z. Yan, Higher-order topological odd-parity superconductors, *Phys. Rev. Lett.* **123**, 177001 (2019).
- [61] K. Laubscher, D. Chughtai, D. Loss, and J. Klinovaja, Kramers pairs of majorana corner states in a topological insulator bilayer, *Phys. Rev. B* **102**, 195401 (2020).
- [62] C. Zeng, T. D. Stanescu, C. Zhang, V. W. Scarola, and S. Tewari, Majorana corner modes with solitons in an attractive Hubbard-Hofstadter model of cold atom optical lattices, *Phys. Rev. Lett.* **123**, 060402 (2019).
- [63] X. Zhu, Second-order topological superconductors with mixed pairing, *Phys. Rev. Lett.* **122**, 236401 (2019).
- [64] N. Bultinck, B. A. Bernevig, and M. P. Zaletel, Three-dimensional superconductors with hybrid higher-order topology, *Phys. Rev. B* **99**, 125149 (2019).
- [65] R.-X. Zhang, W. S. Cole, and S. Das Sarma, Helical hinge majorana modes in iron-based superconductors, *Phys. Rev. Lett.* **122**, 187001 (2019).
- [66] R.-X. Zhang, W. S. Cole, X. Wu, and S. Das Sarma, Higher-order topology and nodal topological superconductivity in Fe(Se,Te) heterostructures, *Phys. Rev. Lett.* **123**, 167001 (2019).
- [67] Z. Wu, Z. Yan, and W. Huang, Higher-order topological superconductivity: Possible realization in fermi gases and  $\text{Sr}_2\text{RuO}_4$ , *Phys. Rev. B* **99**, 020508 (2019).
- [68] S. A. A. Ghorashi, X. Hu, T. L. Hughes, and E. Rossi, Second-order Dirac superconductors and magnetic field induced Majorana hinge modes, *Phys. Rev. B* **100**, 020509 (2019).
- [69] Z. Yan, Majorana corner and hinge modes in second-order topological insulator/superconductor heterostructures, *Phys. Rev. B* **100**, 205406 (2019).
- [70] Z.-R. Liu, L.-H. Hu, C.-Z. Chen, B. Zhou, and D.-H. Xu, Topological excitonic corner states and nodal phase in bilayer quantum spin hall insulators, *Phys. Rev. B* **103**, L201115 (2021).
- [71] Y.-T. Hsu, W. S. Cole, R.-X. Zhang, and J. D. Sau, Inversion-protected higher-order topological superconductivity in monolayer  $\text{WTe}_2$ , *Phys. Rev. Lett.* **125**, 097001 (2020).
- [72] X. Wu, W. A. Benalcazar, Y. Li, R. Thomale, C.-X. Liu, and J. Hu, Boundary-obstructed topological high- $t_c$  superconductivity in iron pnictides, *Phys. Rev. X* **10**, 041014 (2020).
- [73] M. Kheirkhah, Z. Yan, Y. Nagai, and F. Marsiglio, First- and second-order topological superconductivity and temperature-driven topological phase transitions in the extended Hubbard model with spin-orbit coupling, *Phys. Rev. Lett.* **125**, 017001 (2020).
- [74] K. Laubscher, D. Loss, and J. Klinovaja, Majorana and parafermion corner states from two coupled sheets of bilayer graphene, *Phys. Rev. Research* **2**, 013330 (2020).
- [75] Y.-J. Wu, J. Hou, Y.-M. Li, X.-W. Luo, X. Shi, and C. Zhang, In-plane zeeman-field-induced majorana corner and hinge modes in an  $s$ -wave superconductor heterostructure, *Phys. Rev. Lett.* **124**, 227001 (2020).
- [76] J. Ahn and B.-J. Yang, Higher-order topological superconductivity of spin-polarized fermions, *Phys. Rev. Research* **2**, 012060 (2020).
- [77] B. Roy, Higher-order topological superconductors in  $\mathcal{P}$ -,  $\mathcal{T}$ -odd quadrupolar Dirac materials, *Phys. Rev. B* **101**, 220506 (2020).
- [78] S. A. A. Ghorashi, T. L. Hughes, and E. Rossi, Vortex and surface phase transitions in superconducting higher-order topological insulators, *Phys. Rev. Lett.* **125**, 037001 (2020).
- [79] A. Tiwari, A. Jahin, and Y. Wang, Chiral Dirac superconductors: Second-order and boundary-obstructed topology, *Phys. Rev. Research* **2**, 043300 (2020).
- [80] B. Fu, Z.-A. Hu, C.-A. Li, J. Li, and S.-Q. Shen, Chiral Majorana hinge modes in superconducting Dirac materials, *Phys. Rev. B* **103**, L180504 (2021).
- [81] M. Kheirkhah, Y. Nagai, C. Chen, and F. Marsiglio, Majorana corner flat bands in two-dimensional second-order topological superconductors, *Phys. Rev. B* **101**, 104502 (2020).
- [82] S. Ikegaya, W. B. Rui, D. Manske, and A. P. Schnyder, Tunable Majorana corner modes in noncentrosymmetric superconductors: Tunneling spectroscopy and edge imperfections, *Phys. Rev. Research* **3**, 023007 (2021).
- [83] B. Roy and V. Juričić, Mixed-parity octupolar pairing and corner Majorana modes in three dimensions, *Phys. Rev. B* **104**, L180503 (2021).
- [84] S. Qin, C. Fang, F.-C. Zhang, and J. Hu, Topological superconductivity in an extended  $s$ -wave superconductor and its implication to iron-based superconductors, *Phys. Rev. X* **12**, 011030 (2022).
- [85] H. D. Scammell, J. Ingham, M. Geier, and T. Li, Intrinsic first- and higher-order topological superconductivity in a doped topological insulator, *Phys. Rev. B* **105**, 195149 (2022).
- [86] S.-Q. Shen, [Topological insulators](#), Vol. 174 (Springer, 2012).
- [87] B. A. Bernevig, Topological insulators and topological superconductors, in [Topological Insulators and Topological Superconductors](#) (Princeton university press, 2013).
- [88] M.-X. Wang, C. Liu, J.-P. Xu, F. Yang, L. Miao, M.-Y. Yao, C. Gao, C. Shen, X. Ma, X. Chen, et al., The coexistence of superconductivity and topological order in the  $\text{Bi}_2\text{Se}_3$  thin films, *Science* **336**, 52 (2012).
- [89] S.-Y. Xu, N. Alidoust, I. Belopolski, A. Richardella, C. Liu, M. Neupane, G. Bian, S.-H. Huang, R. Sankar, C. Fang, et al., Momentum-space imaging of cooper pairing in a half-dirac-gas topological superconductor, *Nature Physics* **10**, 943 (2014).
- [90] J.-P. Xu, C. Liu, M.-X. Wang, J. Ge, Z.-L. Liu, X. Yang, Y. Chen, Y. Liu, Z.-A. Xu, C.-L. Gao, D. Qian, F.-C. Zhang, and J.-F. Jia, Artificial topological superconductor by the proximity effect, *Phys. Rev. Lett.* **112**, 217001 (2014).
- [91] L. Fu and C. L. Kane, Superconducting proximity effect and majorana fermions at the surface of a topological insulator, *Phys. Rev. Lett.* **100**, 096407 (2008).

- [92] C.-X. Liu and B. Trauzettel, Helical dirac-majorana interferometer in a superconductor/topological insulator sandwich structure, *Phys. Rev. B* **83**, 220510 (2011).
- [93] H.-H. Sun, K.-W. Zhang, L.-H. Hu, C. Li, G.-Y. Wang, H.-Y. Ma, Z.-A. Xu, C.-L. Gao, D.-D. Guan, Y.-Y. Li, C. Liu, D. Qian, Y. Zhou, L. Fu, S.-C. Li, F.-C. Zhang, and J.-F. Jia, Majorana zero mode detected with spin selective andreev reflection in the vortex of a topological superconductor, *Phys. Rev. Lett.* **116**, 257003 (2016).
- [94] Y. Zhang, K. He, C.-Z. Chang, C.-L. Song, L.-L. Wang, X. Chen, J.-F. Jia, Z. Fang, X. Dai, W.-Y. Shan, S.-Q. Shen, Q. Niu, X.-L. Qi, S.-C. Zhang, X.-C. Ma, and Q.-K. Xue, Erratum: Crossover of the three-dimensional topological insulator  $\text{Bi}_2\text{Se}_3$  to the two-dimensional limit, *Nature Physics* **6**, 712 (2010).
- [95] M. J. Park, Y. Kim, G. Y. Cho, and S. Lee, Higher-order topological insulator in twisted bilayer graphene, *Phys. Rev. Lett.* **123**, 216803 (2019).
- [96] T. Liu, Y.-R. Zhang, Q. Ai, Z. Gong, K. Kawabata, M. Ueda, and F. Nori, Second-order topological phases in non-hermitian systems, *Phys. Rev. Lett.* **122**, 076801 (2019).
- [97] R. Jackiw and C. Rebbi, Solitons with fermion number  $1/2$ , *Phys. Rev. D* **13**, 3398 (1976).
- [98] M. V. Berry, Quantal phase factors accompanying adiabatic changes, *Proceedings of the Royal Society of London. A. Mathematical and Physical Sciences* **392**, 45 (1984).
- [99] F. Wilczek and A. Zee, Appearance of gauge structure in simple dynamical systems, *Phys. Rev. Lett.* **52**, 2111 (1984).
- [100] A. Alexandradinata, X. Dai, and B. A. Bernevig, Wilson-loop characterization of inversion-symmetric topological insulators, *Phys. Rev. B* **89**, 155114 (2014).
- [101] X.-W. Luo and C. Zhang, Higher-order topological corner states induced by gain and loss, *Phys. Rev. Lett.* **123**, 073601 (2019).
- [102] C.-X. Liu, H. Zhang, B. Yan, X.-L. Qi, T. Frauenheim, X. Dai, Z. Fang, and S.-C. Zhang, Oscillatory crossover from two-dimensional to three-dimensional topological insulators, *Phys. Rev. B* **81**, 041307 (2010).